BUTTERWORTH HEINEMANN

Investigation of multiple-time-scale Reynolds stress model in homogeneous anisotropic turbulence

M. Yamamoto
Department of Mechanical Engineering, Science University of Tokyo, Kagurazaka, Shinjuku-ku, Tokyo, Japan

A multiple-time-scale Reynolds stress model is proposed to extend universality and to overcome the defect introduced by the single-time-scale nature generally adopted in conventional turbulence models. Using grid turbulence and homogeneous shear flow, the model coefficients associated with (for the most part) pressure–strain correlation are determined analytically and/or numerically. The model performance is verified for a wide variety of flows subject to varying conditions. Comparing my numerical results with corresponding experimental data, it is shown that the present model can satisfactorily reproduce the change of each Reynolds stress component

Keywords: turbulent flow; Reynolds stress model; multiple-time-scale; pressure–strain correlation

Introduction

Although many turbulence models have been developed and used in various engineering applications, no single model is able to predict all kinds of turbulent flows. It is, therefore, important to construct a more universally valid model of turbulence.

Conventional turbulence models describe turbulent flow characterized by a single-time-scale, which generally is determined by the turbulent kinetic energy k and its dissipation rate ε (more precisely, by the ratio k/ε). Using this single-time-scale nature implicitly assumes that the shape of a turbulent kinetic energy spectrum is universal. However, this assumption is not always valid for many types of turbulent flows. Therefore, these models cannot predict flows displaying turbulent behavior of differing time-scales or whose turbulent energy spectrums change drastically. To overcome this defect, Hanjalic et al. (1980) proposed a multiple-time-scale model. They divided the turbulent kinetic energy spectrum into three parts (the production, transfer, and dissipation regions) and constructed a two-time-scale k-ε model. By applying the model to the cases of grid turbulence produced through a sudden contraction, jet, and boundary layers in adverse pressure gradients, it was reported that the model yields considerably improved results. Wilcox (1986, 1988) developed a two-time-scale k-ω model and obtained solutions better than those obtained from single-time-scale k-ω models for both incompressible and compressible flows. Kim et al. (1987, 1988, 1989, 1991) extended Hanjalic's model and successfully applied it to certain kinds of wall shear flows. However, since these models contain an eddy viscosity hypothesis, it cannot be expected that they are significantly more universal than a single-time-scale Reynolds stress model. A multiple-time-scale Reynolds stress model has also been investigated. Based on the work performed by Jeandel et al. (1978), Schiestel (1987) derived and modeled multiple-time-scale Reynolds stress transport equations. However, the validity of these equations has not been verified for several types of flows. Further investigation of multiple-time-scale Reynolds stress models is needed.

In this study, the basic forms of the model equations governing the transport phenomena of Reynolds stresses and energy transfer rates within each partitioned energy spectral slice are introduced. These equations are applied to grid turbulence and homogeneous shear flow to determine the model coefficients, mainly related to pressure–strain correlation. In addition, the model performance is verified using a significant amount of experimental data under varying conditions. The results show that the present model can satisfactorily reproduce the behavior of each Reynolds stress component.

Basic equations of multiple-time-scale Reynolds stress model

Reynolds stress transport equations

In a multiple-time-scale model, the turbulent kinetic energy spectrum is decomposed into several parts, and the phenomena within each spectral slice are considered. Therefore, a variable is divided as follows:

$$\tilde{f} = \bar{f} + f^{(1)} + f^{(2)} + f^{(3)} + , \ldots , = \bar{f} + \sum_{m} f^{(m)} \tag{1}$$

Substituting this decomposition into the Navier–Stokes equation, after some algebra, the Reynolds stress can be obtained as follows:

$$R_{ij} = \overline{u_i u_j} = \sum_{m=n} \overline{u_i^{(m)} u_j^{(n)}} + \sum_{m \neq n} \overline{u_i^{(m)} u_j^{(n)}} \tag{2}$$

Hence, turbulent stress is expressed by the interactions within a spectral slice and those between different scales. Comparing this

Address reprint requests to Prof. M. Yamamoto, Department of Mechanical Engineering, Science University of Tokyo, 1-3 Kagurazaka, Shinjuku-ku, Tokyo, Japan

Received 1 February 1995; accepted 30 May 1995

Int. J. Heat and Fluid Flow 16: 417–428, 1995

655 Avenue of the Americas, New York, NY 10010

0142-727X/95/$10.00
SSDI 0142-727X(95)00045-R

expression with that used in large-eddy simulations (LES), the former term corresponds to the Reynolds term and the latter to the sum of cross and Leonard terms. It is well known that cross and Leonard terms mutually cancel, and thus, neglecting these terms does not affect the numerical results. Furthermore, the presence of too many variables makes it difficult to determine model coefficients. With these points in mind, I neglected interactions between different scales in the present study. Therefore, the Reynolds stress becomes:

$$R_{ij} = \sum_{m=n} \overline{u_i^{(m)} u_j^{(n)}} \tag{3}$$

and only the transport equation for each $R_{ij}^{(m)}$ individually needs to be treated.

By taking the Fourier transformation of two-point fluctuating velocity correlation equations and integrating over the (m)th spectral slice, we can derive transport equations of the Reynolds stress $R_{ij}^{(m)}(=\overline{u_i^{(m)} u_j^{(m)}})$ in this slice (Schiestel 1987).

$$\frac{DR_{ij}^{(m)}}{Dt} = P_{ij}^{(m)} + T_{ij}^{(m-1)} - T_{ij}^{(m)} + \Phi_{ij}^{(m)} + D_{ij}^{(m)} - \varepsilon_{ij}^{(m)} \tag{4}$$

where

$$P_{ij}^{(m)} = -R_{kj}^{(m)} \frac{\partial U_i}{\partial x_k} - R_{ik}^{(m)} \frac{\partial U_j}{\partial x_k} \tag{5}$$

$$T_{ij}^{(m)} = \int_0^{\kappa(m)} \int \frac{\partial}{\partial \xi_k} \left(\overline{u_{Ai} u_{Bj} u_{Ak}} - \overline{u_{Ai} u_{Bj} u_{Bk}} \right) \mathrm{d}S \, \mathrm{d}\kappa$$

$$- \phi_{ij}(\kappa(m)) \frac{D\kappa(m)}{Dt}$$

$$+ \frac{1}{2} \int_0^{\kappa(m)} \int R_{ik} \xi_m \, \mathrm{d}S \, \mathrm{d}\kappa \frac{\partial^2 U_j}{\partial x_k \partial x_m}$$

$$- \frac{1}{2} \int_0^{\kappa(m)} \int R_{kj} \xi_m \, \mathrm{d}S \, \mathrm{d}\kappa \frac{\partial^2 U_i}{\partial x_k \partial x_m}$$

$$+ \int_0^{\kappa(m)} \int \xi_m \frac{\partial R_{ij}}{\partial \xi_k} \, \mathrm{d}S \, \mathrm{d}\kappa \frac{\partial U_k}{\partial x_m} \tag{6}$$

$$\Phi_{ij}^{(m)} = \frac{2}{\rho} \int_{\kappa(m-1)}^{\kappa(m)} \int \left(\overline{p_A \frac{\partial u_{Bj}}{\partial \xi_i}} - \overline{p_B \frac{\partial u_{Ai}}{\partial \xi_j}} \right) \mathrm{d}S \, \mathrm{d}\kappa \tag{7}$$

$$D_{ij}^{(m)} = -\frac{1}{2} \frac{\partial}{\partial x_k} \int_{\kappa(m-1)}^{\kappa(m)} \int \left(\overline{u_{Ai} u_{Bj} u_{Ak}} + \overline{u_{Ai} u_{Bj} u_{Bk}} \right) \mathrm{d}S \, \mathrm{d}\kappa$$

$$- \frac{1}{\rho} \frac{\partial}{\partial x_i} \int_{\kappa(m-1)}^{\kappa(m)} \int \overline{p_A u_{Bj}} \, \mathrm{d}S \, \mathrm{d}\kappa$$

$$+ \frac{1}{\rho} \frac{\partial}{\partial x_j} \int_{\kappa(m-1)}^{\kappa(m)} \int \overline{p_B u_{Ai}} \, \mathrm{d}S \, \mathrm{d}\kappa + \nu \frac{\partial^2 R_{ij}^{(m)}}{\partial x_k^2} \tag{8}$$

$$\varepsilon_{ij}^{(m)} = -8\nu \int_{\kappa(m-1)}^{\kappa(m)} \int \overline{\frac{\partial u_{Ai}}{\partial \xi_k} \frac{\partial u_{Bj}}{\partial \xi_k}} \, \mathrm{d}S \, \mathrm{d}\kappa \tag{9}$$

The terms here represent total time derivative (i.e., temporal change plus convection), production, energy transfer from $(m\text{-}1)$th to (m)th spectral slice, energy transfer from (m)th to $(m+1)$th spectral slice, redistribution, diffusion, and dissipation, respectively. The temporal change, convection and production terms can be handled exactly, but the remaining terms have to be modeled.

Energy transfer rate equations

The most remarkable difference between single- and multiple-time-scale models is the treatment of energy transfer. Single-time-scale models assume that energy transfer is constant over the spectral space and is identical to the dissipation rate of turbulent kinetic energy. Hence, the energy transfer does not appear explicitly in the model equations.

Although it may be possible to derive exact transport equations for energy transfer rates from Navier–Stokes equations, it is not presently realistic. Schiestel (1987) proposed transport equations for $T^{(m)}(=\frac{1}{2}T_{kk}^{(m)})$ extending the work of Jeandel et al.

Notation

a_{ij}	anisotropy tensor of R_{ij}, $R_{ij}/e - 2/3\delta_{ij}$
$a_{T_{ij}}$	anisotropy tensor of T_{ij}, $T_{ij}/T - 2/3\delta_{ij}$
C_i, α_i	model coefficients
D_{ij}	diffusion
$\int \mathrm{d}S$	surface integration over sphere of radius κ
$\int \mathrm{d}\kappa$	integration over wave number κ
k, e	turbulent kinetic energy, $1/2R_{ii}$
P_{ij}	production
p	fluctuating pressure
R_{ij}	Reynolds stress, $\overline{u_i u_j}$
r	ratio of turbulent kinetic energies, $e^{(2)}/e^{(1)}$
S_{ij}	mean strain rate
s	ratio of anisotropic tensor, $a_{ij}^{(2)}/a_{ij}^{(1)}$
T_{ij}	energy transfer rate
t	time
U_i	mean velocity component
u_i	fluctuating velocity component
x_i	Cartesian coordinate
II	second invariant of anisotropy tensor, $a_{ij}a_{ji}$
III	third invariant of anisotropy tensor, $a_{ij}a_{jk}a_{ki}$

Greek

β	ratio of energy transfer rates, $T^{(2)}/T^{(1)}$
β', β''	integral constant
δ_{ij}	Kronecker's delta
ε	dissipation rate of total turbulent kinetic energy
ε_{ij}	dissipation
κ	wave number
ν	kinematic viscosity
Φ_{ij}	pressure-strain correlation
ϕ_{ij}	surface integration of 2-point velocity correlation, $\int (u_i)_A (u_j)_B \, \mathrm{d}S$
ω_{ij}	mean vorticity

Superscript

(m)	value in the mth spectral slice

Subscripts

A, B	different points with a displacement ξ
R	rapid part of pressure–strain correlation
S	slow part of pressure–strain correlation
T	energy transfer rate

(1978). However, since he assumed a $-5/3$ law for the energy spectrum, isotropic turbulence, and proportionality of $T_{ij}^{(m)}$ and $T^{(m)}R_{ij}^{(m)}/e^{(m)}$ in his modeling process, the model equations lack universality despite their complex forms. Seeking a more universally valid model, I set out to construct transport equations for energy transfer rates by following the intuitive approach introduced in early works concerned with modeling of the dissipation rate equation. Introducing the time constant $e^{(m)}/T^{(m)}$ and model coefficients into the Reynolds stress transport equations, the transport equations for energy transfer rates in the (m)th spectral slice can be expressed as follows:

$$\frac{DT_{ij}^{(m)}}{Dt} = \alpha_1^{(m)}\frac{T^{(m)}}{e^{(m)}}P_{ij}^{(m)} + \alpha_2^{(m)}\frac{T^{(m)}}{e^{(m)}}T_{ij}^{(m-1)} - \alpha_3^{(m)}\frac{T^{(m)}}{e^{(m)}}T_{ij}^{(m)} + \Phi_{T_{ij}}^{(m)} + D_{T_{ij}}^{(m)} - \varepsilon_{T_{ij}}^{(m)} \tag{10}$$

Each term here represents the same quantity as the corresponding term in the Reynolds stress equation. It should be noted that energy transfer to the first spectral slice does not exist (i.e., $T_{ij}^{(0)} = 0$), and the rate of energy transfer to the last spectral slice is equal to the dissipation rate of turbulent kinetic energy (i.e., $T^{(n)} = \varepsilon$) when the turbulent Reynolds number is sufficiently large.

Grid turbulence

Model equations

A two-time-scale model is probably the most useful in practical applications because of the relatively short computation time. Therefore, I treat a two-time-scale Reynolds stress model in the present study. In this model, the energy spectrum is decomposed into three parts (i.e., low, intermediate, and high wave number regions). Below, I refer to the low wave number region ($m = 1$) as the "large-scale" and the middle one ($m = 2$) as the "small-scale."

The pressure–strain term in a multiple-time-scale Reynolds stress transport equation is similar to that in the single-time-scale case. This term consists of slow, rapid, and wall terms (Schiestel 1987). Therefore, such a model, valid in a single-time-scale model, can be used in a multiple-time-scale model in principle. To reproduce the nonlinear behavior of turbulence, I borrowed from a generalized model (Lumley and Newman 1977) for the slow term in pressure–strain correlation. Then, model equations for grid turbulence are expressed as follows:

$$\frac{dR_{ij}^{(m)}}{dt} = T_{ij}^{(m-1)} - T_{ij}^{(m)} - C_1^{(m)}T^{(m)}a_{ij}^{(m)} + C_2^{(m)}T^{(m)}\left(a_{ik}^{(m)}a_{kj}^{(m)} - \frac{1}{3}II^{(m)}\delta_{ij}\right) \tag{11}$$

$$\frac{dT_{ij}^{(m)}}{dt} = \alpha_2^{(m)}\frac{T^{(m)}}{e^{(m)}}T_{ij}^{(m-1)} - \alpha_3^{(m)}\frac{T^{(m)}}{e^{(m)}}T_{ij}^{(m)} - \alpha_4^{(m)}\frac{T^{(m)}T^{(m)}}{e^{(m)}}a_{T_{ij}}^{(m)} + \alpha_5^{(m)}\frac{T^{(m)}T^{(m)}}{e^{(m)}}\left(a_{T_{ik}}^{(m)}a_{T_{kj}}^{(m)} - \frac{1}{3}II_T^{(m)}\delta_{ij}\right) \tag{12}$$

However, because small-scale turbulence is not expected to be highly anisotropic, a linear equation should be sufficient in describing small-scale behavior (i.e., $C_2^{(2)} = \alpha_5^{(2)} = 0$). Also, $\alpha_2^{(1)}$ has no meaning, because $T_{ij}^{(0)} = 0$.

Determination of model coefficients

Coefficients $\alpha_3^{(m)}$ and $\alpha_2^{(m)}$. The coefficients $\alpha_3^{(m)}$ and $\alpha_2^{(m)}$ were determined using experimental data for the decay rate of grid turbulence. Contracting Equations 11 and 12, we obtain the following equations.

$$\frac{de^{(1)}}{dt} = -T^{(1)} \tag{13}$$

$$\frac{de^{(2)}}{dt} = T^{(1)} - T^{(2)} \tag{14}$$

$$\frac{dT^{(1)}}{dt} = -\alpha_3^{(1)}\frac{T^{(1)}}{e^{(1)}}T^{(1)} \tag{15}$$

$$\frac{dT^{(2)}}{dt} = \alpha_2^{(2)}\frac{T^{(2)}}{e^{(2)}}T^{(1)} - \alpha_3^{(2)}\frac{T^{(2)}}{e^{(2)}}T^{(2)} \tag{16}$$

where $T^{(2)}$ is equal to the dissipation rate ϵ.

First, let us consider the situation relatively far downstream from the grid. In this region, it is expected that the ratio of large-scale to small-scale energy [i.e., $r = e^{(2)}/e^{(1)}$] approaches a certain asymptotic value (Kim and Chen 1987), and the turbulent Reynolds number is still large. Defining the total turbulent kinetic energy as $e = e^{(1)} + e^{(2)}$, the following equations can be derived.

$$e^{(1)} = \frac{1}{1+r}e, \qquad e^{(2)} = \frac{r}{1+r}e \tag{17}$$

Substituting these relations into Equations 13 and 14, after some algebra, we obtain:

$$\frac{T^{(2)}}{T^{(1)}} = 1 + r \tag{18}$$

Thus, the ratio of energy transfer rates becomes constant.

Using the above relations and arranging Equations 13 and 15, we can derive an expression for the temporal change of the total turbulent kinetic energy e.

$$e = \beta' t^{-1/(\alpha_3^{(1)}-1)} \tag{19}$$

Next, let us consider the situation much further downstream from the grid (i.e., the terminal stage of decaying turbulence). In this region, it can be assumed that the contribution from large-scale motion is relatively small and that the turbulent Reynolds number is small. Thus, by neglecting these contributions in Equations 14 and 16, we can obtain the following expression for e.

$$e = \beta'' t^{-1/(\alpha_3^{(2)}-1)} \tag{20}$$

Many experiments indicate that $1/(\alpha_3^{(m)} - 1)$ takes values in the range $1.0 \sim 1.25$ at high turbulent Reynolds numbers and approximately 2.5 at low turbulent Reynolds numbers. I adopted the values 1.25 and 2.5 for the respective situations. Thus,

$$\alpha_3^{(1)} = 1.8, \qquad \alpha_3^{(2)} = 1.4 \tag{21}$$

Following similar steps for the contracted equations, the expression relating $\alpha_3^{(1)}$, $\alpha_3^{(2)}$, and $\alpha_2^{(2)}$ can be derived

$$\alpha_2^{(2)} = (1+r)\alpha_3^{(2)} - r\alpha_3^{(1)} \tag{22}$$

The asymptotic value of the energy ratio $r(= e^{(2)}/e^{(1)})$ depends on the partitioning wave number. I set $r = 1.5$, following the study of Kim and Chen (1987). Therefore, Equation 21 and 22 leads to:

$$\alpha_2^{(2)} = 0.8 \tag{23}$$

However, these coefficients are not constant, but rather depend on the spectral shape. Hanjalic et al. (1980) and Kim and Chen (1987) proposed that the energy transfer from large-scale to small-scale increases when the energy ratio r is made small. In

this study, I consider both $\alpha_3^{(1)}$ and $\alpha_2^{(2)}$ as functions of r. The functional forms were determined by computational optimization under the following four constraints: (1) They reproduce the experimental data measured by Makita et al. (1993) under highly anisotropic conditions; (2) the energy ratio r increases monotonically during the decay; (3) r approaches 1.5; and (4) they attain the proper asymptotic values (i.e., 1.8 and 0.8, respectively). With these constraints in mind, I adopted following functional forms.

$$\alpha_3^{(1)} = 1.8 \min(1.0, r), \qquad \alpha_3^{(2)} = 1.4,$$
$$\alpha_2^{(2)} = 0.8 - 0.25(r - 1.5) \tag{24}$$

Coefficients $C_1^{(m)}$ and $C_2^{(m)}$. These coefficients were determined by use of realizability conditions (Schumann 1977) in each spectral slice. First, let us consider the situation where the influence of the initial state is negligible. Then turbulence is nearly isotropic, and the nonlinear effect of $a_{ij}^{(1)}$ can be neglected. In addition, energy transfer rates $T_{ij}^{(1)}$ are expected to be isotropic. Therefore, Equation 11 with $m = 1$ reduces to

$$\frac{dR_{kk}^{(1)}}{dt} = -\frac{2}{3}T^{(1)} - C_1^{(1)}T^{(1)}a_{kk}^{(1)} = 0 \quad \text{(no summation over } k\text{)} \tag{25}$$

Using a realizability constraint ($R_{ij}^{(1)} \to 0$, and therefore $a_{kk}^{(1)} \to -2/3$), this equation yields $C_1^{(1)} = 1.0$.

Similarly, using Equation 11 with $m = 2$ and Equation 18, the following equation can be derived.

$$C_1^{(2)} = \frac{T^{(2)} - T^{(1)}}{T^{(2)}} = \frac{r}{1+r} \tag{26}$$

Assuming the asymtotic value $r = 1.5$, we obtain

$$C_1^{(2)} = 0.6 \tag{27}$$

Next, let us consider the situation where the turbulence is strongly anisotropic, and the nonlinear effect cannot be neglected. Then $C_1^{(1)}$ is expected to be larger than the asymptotic value 1.0 and should assume values in the range $1.5 \sim 1.8$, as seen in the case of successful study of single-time-scale Reynolds stress models (e.g., Launder et al. 1975). In addition, as was found in the computational optimization of the functions $\alpha_3^{(1)}$ and $\alpha_2^{(2)}$, existing experimental data put the value of r around $r = 0.6$. Considering these two points, the following functional form was adopted.

$$C_1^{(1)} = 1.0 + \frac{0.3}{r} \tag{28}$$

In addition, for $m = 1$, Equation 11 reduces to

$$\frac{dR_{kk}^{(1)}}{dt} = -T_{kk}^{(1)} - C_1^{(1)}T^{(1)}a_{kk}^{(1)} + C_2^{(1)}T^{(1)}\left(a_{kk}^{(1)}a_{kk}^{(1)} - \frac{1}{3}II^{(1)}\right) = 0 \tag{29}$$

Since the anisotropy of the energy transfer rates depends on that of the Reynolds stresses in a highly fluctuating flow, it can be assumed that the anisotropy of $T_{ij}^{(1)}$ is the same as that of $R_{ij}^{(1)}$. Using this assumption, Equation 29 becomes

$$\frac{dR_{kk}^{(1)}}{dt} = -\left(a_{kk}^{(1)} + \frac{2}{3}\right)T^{(1)} - C_1^{(1)}T^{(1)}a_{kk}^{(1)} + C_2^{(1)}T^{(1)}\left(a_{kk}^{(1)}a_{kk}^{(1)} - \frac{1}{3}II^{(1)}\right) = 0 \tag{30}$$

Applying the realizability condition to this equation, we obtain

$$C_1^{(1)} + C_2^{(1)}\left(\frac{2}{3} - \frac{1}{2}II^{(1)}\right) = 0 \tag{31}$$

As the equality must be satisfied when $II^{(1)}$ is maximum, Equation 31 gives

$$C_2^{(1)} = 1.5C_1^{(1)} \tag{32}$$

Coefficients $\alpha_4^{(m)}$ and $\alpha_5^{(m)}$. Since there is apparently no accessible way to obtain these coefficients analytically, I determined them by computational optimization. The computations were performed using the experimental data measured by Makita et al. (1993) with an initially positive third invariant *III*. The following six constraints were imposed: (1) the coefficient values are able to reproduce the experimental data; (2) the energy ratio r increases monotonically; (3) r approaches 1.5 asymptotically; (4) the $R_{ij}^{(m)}$ do not intersect one another during the decay; (5) the $T_{ij}^{(m)}$ do not intersect; and (6) the second invariant *II* decreases monotonically. Under these constraints, I adopted the following:

$$\alpha_4^{(1)} = 1.6C_1^{(1)}, \qquad \alpha_4^{(2)} = 2.5, \qquad \alpha_5^{(1)} = 1.6 \tag{33}$$

Initial conditions and numerical method

The method to set initial conditions is crucial for a multiple-time-scale turbulence model. In the present study, I set initial values on the basis of the following assumptions.

The first assumption is that the anisotropy of small-scale turbulence is proportional to that of large-scale turbulence. Thus, $a_{ij}^{(2)} = sa_{ij}^{(1)}$. This assumption leads Reynolds stress components in each spectral slice as follows:

$$R_{ij}^{(1)} = \left(\frac{1+r}{1+rs}a_{ij} + \frac{2}{3}\delta_{ij}\right)\frac{1}{1+r}e \tag{34}$$

$$R_{ij}^{(2)} = \left(\frac{1+r}{1+rs}sa_{ij} + \frac{2}{3}\delta_{ij}\right)\frac{r}{1+r}e \tag{35}$$

The second assumption is that in each spectral slice energy transfer rates have the same anisotropy as do the Reynolds stresses. This assumption gives:

$$T_{ij}^{(1)} = \left(\frac{1+r}{1+rs}a_{ij} + \frac{2}{3}\delta_{ij}\right)\frac{T^{(2)}}{\beta} \tag{36}$$

$$T_{ij}^{(2)} = \left(\frac{1+r}{1+rs}sa_{ij} + \frac{2}{3}\delta_{ij}\right)T^{(2)} \tag{37}$$

It is expected that the sensitivities of s and β to r are dependent on the state of turbulence. For typical cases, these take values; $r = 1.5$, $s = 0.0$, $\beta = 2.5$ for asymptotic grid turbulence, $r = 0.25$, $\beta = 1.0$ for turbulent boundary layers (Kim and Chen 1987), and $s = 1.0$ for $r = 0.0$. Considering these conditions, I made s and β assume the following functional dependence on the energy ratio r.

$$s = \exp(-2.0r^2), \qquad \beta = 1.2r + 0.7 \tag{38}$$

Computations were performed through the following four steps. *Step I.* As $T^{(2)} = \varepsilon$, an initial $T^{(2)}$ is calculated with the use of a standard $k-\varepsilon$ model. *Step II.* Solving the contracted Equations 13–16, an initial energy ratio r is estimated. *Step III.* Using Equations 34–38, initial conditions of $R_{ij}^{(m)}$ and $T_{ij}^{(m)}$ are calculated. *Step IV.* Solving Equations 11 and 12, the temporal changes of all variables are calculated.

A fourth-order Runge–Kutta method was used in all simulations. The time step was set to such a value that the terminal time was reached in each case after 200 time steps. It should be noted that, although I calculated the same flows using time steps half this size, the maximum difference in the Reynolds stresses was only 0.7%.

Results and discussion

I considered six sets of experimental data. The data obtained by Makita et al. (1993), Le Penven et al. (1985), and Gence and Mathieu (1979) show a positive third invariant. These data indicate that nonlinearity exists when the third invariant is positive and becomes stronger with the increase of anisotropy. The remaining three cases measured by Makita et al., Le Penven et al., and Tucker and Reynolds (1968) show a negative third invariant initially. The data by Makita et al. indicate that nonlinear behavior is exhibited even when the third invariant is negative, while the second and third sets of data do not exhibit apparent nonlinearlity. Their turbulent Reynolds numbers are large enough to neglect low Reynolds number effects.

My numerical results for the time development of the total turbulent kinetic energy and normal Reynolds stresses and the behavior of the second and third invariants (i.e., invariant map) are compared in the figures with the corresponding experimental data. In addition, the behavior of Reynolds stresses and energy transfer rates in each spectral slice are displayed.

Figures 1–3 depict results for cases with a positive third invariant. Figure 1 shows the results calculated for the experiment performed by Makita et al. (1993). The data shown here are those used in determining the model coefficients. Thus, the numerical results are, not surprisingly, in good agreement with the experiment. Figure 1a shows the time dependence of the total turbulent kinetic energy and total Reynolds stresses. The turbulence initially tends toward axisymmetry and gradually decays. It is evident that the present model can reproduce the nonlinear behavior satisfactorily. This aspect can also be seen in the invariant map (Figure 1b). Figure 1c displays the time dependence of Reynolds stresses in large- and small-scale turbulence. Large-scale motion initially accounts for most of the energy, but as time passes, the energy becomes more evenly distributed among scales through the decay. In addition, large-scale motion becomes axisymmetric rapidly, and small-scale motion tends toward axisymmetry as it is influenced by the large-scale motion, although small-scale equations do not include nonlinear terms. It is very interesting that the small-scale turbulent behavior is governed by that on large-scales. Figure 1d shows the temporal changes of the energy transfer rates. The results show that energy transfer rates become axisymmetric initially, and they behave in a manner similar to the Reynolds stress components. However, the energy transfer rates become isotropic more quickly than do Reynolds stresses. In existing single-time-scale models, it is generally assumed that the energy transfer rate is equal to the dissipation rate and that it is isotropic. Thus, the present model supports this hypothesis in the case of turbulence with weak anisotropy.

Figures 2 and 3 show the results for the experiments performed by Le Penven et al. (1985) and Gence and Mathieu (1979). The results here are similar to those for the experiment by Makita et al. (1993). Numerical results are again in good agreement with the experimental data. The nonlinear behavior is correctly captured. It should be noted that existing single-time-scale models cannot predict this nonlinear behavior satisfactorily (Yamamoto and Arakawa 1991). Although the temporal changes of Reynolds stresses and energy transfer rates in each spectral slice are not shown here, the results indicate that the small-scale energy transfer rates remain anisotropic in the terminal stage.

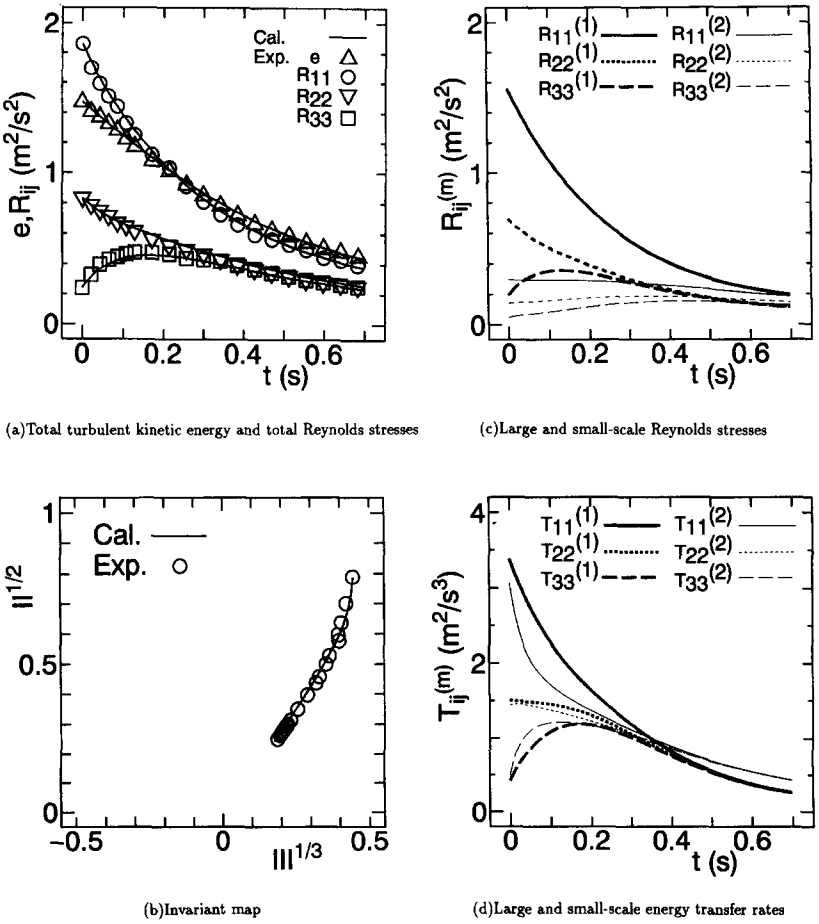

Figure 1 Comparison of numerical results with experiments (data: Makita et al. 1993, $III > 0$)

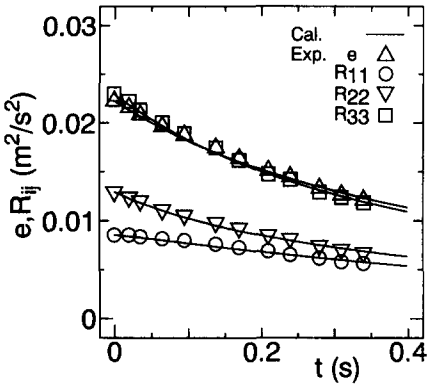

(a)Total turbulent kinetic energy and total Reynolds stresses

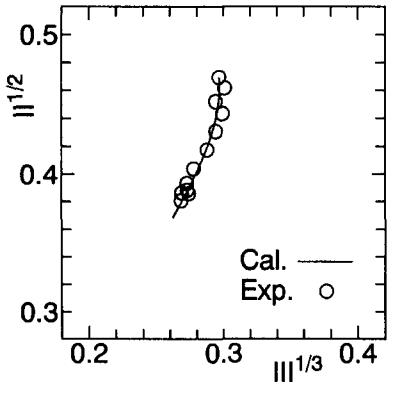

(b)Invariant map

Figure 2 Comparison of numerical results with experiments (data: Le Penven et al. 1985, $III > 0$)

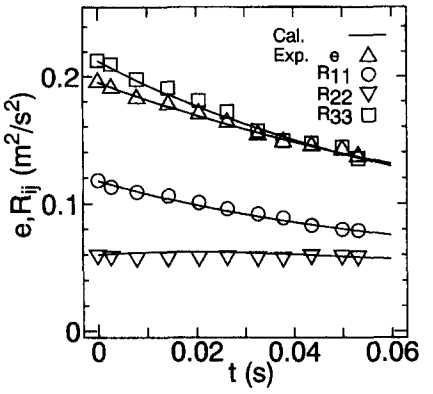

(a)Total turbulent kinetic energy and total Reynolds stresses

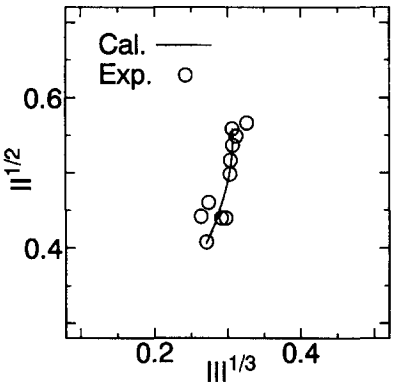

(b)Invariant map

Figure 3 Comparison of numerical results with experiments (data: Gence and Mathieu 1979, $III > 0$)

This fact suggests that these experiments were carried out over a relatively short period.

Next, I consider another three cases with an initially negative third invariant. Figure 4 shows the results for the experiment done by Makita et al. (1993). These data are the most anisotropic among the experiments used in this study. Therefore, a very strong nonlinearlity is shown. It has been thought that the turbulence with an initially negative third invariant evolves toward isotropy linearly (Le Penven et al. 1985). However, these data indicate that turbulence has a strong nonlinear character, even in the case with a negative third invariant, if the anisotropy of turbulence is large enough. Figure 4a shows the time dependence of the total turbulent kinetic energy and total Reynolds stresses. The decay calculated using the present model delays slightly around $t = 0.7$, but the agreement is satisfactory. Makita et al. (1993) noted that initially axisymmetrization takes place and at later times decay becomes dominant. This behavior is reproduced by the present model qualitatively. Figure 4b shows the evolution in a phase space. The numerical results display very strong nonlinearity, but the agreement with the experimental data is not complete. This would be caused by the choice of unsuitable functions for $\alpha_3^{(1)}$ and $\alpha_2^{(2)}$.

The remaining cases with a negative third invariant are the experiments performed by Le Penven et al. (1985) and Tucker and Reynolds (1968). These data are more isotropic than Makita et al.'s (1993) data. Figures 5 and 6 show the results, respectively. The numerical results are in good agreement with the corresponding experiments. The present model apparently has no problem reproducing the results of experiments, except in the case where the turbulence is highly anisotropic. It should be noted that the numerical results show the tendency of the third invariant to change sign. In fact, further calculations showed that the third invariant becomes positive, and the turbulence then evolves toward isotropy.

These computations make it clear that the present model can satisfactorily predict the return to isotropy problems with various states of turbulence. In addition, the temporal changes of both the Reynolds stresses and energy transfer rates are smooth and possess no singularity in all cases. Therefore, it is recognized indirectly that the method used here to set initial conditions is reasonable for a wide range of grid turbulence.

Homogeneous shear flow

Model equations

A rapid term in the pressure–strain correlation plays an important role in flows where a mean velocity gradient exists. Hence, this term is the key to modeling in engineering applications.

According to Speziale et al. (1991), the rapid term model in the pressure–strain correlation can generally be expressed as follows:

$$\Phi_{R_{ij}} = C_1 e S_{ij} + C_2 e\left(a_{ik}S_{jk} + a_{jk}S_{ik} - \frac{2}{3}a_{mn}S_{mn}\delta_{ij}\right) + C_3 e\left(a_{ik}a_{kl}S_{jl} + a_{jk}a_{kl}S_{il} - \frac{2}{3}a_{lm}a_{mn}S_{nl}\delta_{ij}\right) + C_4 e(a_{ik}\omega_{jk} + a_{jk}\omega_{ik}) + C_5 e(a_{ik}a_{kl}\omega_{jl} + a_{jk}a_{kl}\omega_{il}) \quad (39)$$

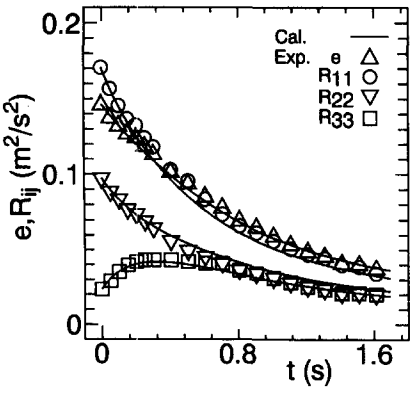

(a)Total turbulent kinetic energy and total Reynolds stresses

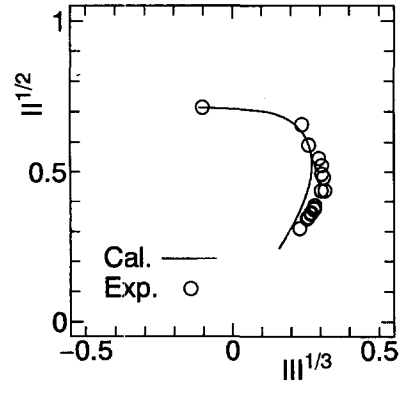

(b)Invariant map

Figure 4 Comparison of numerical results with experiments (data: Makita et al. 1993, $III < 0$ at $t = 0.0$)

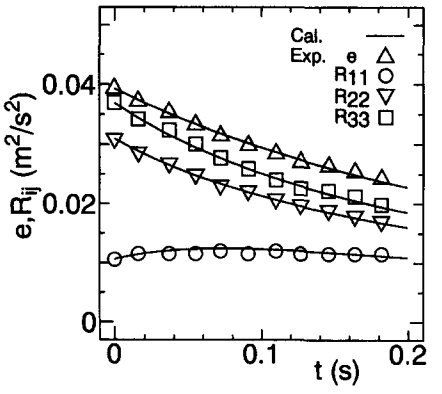

(a)Total turbulent kinetic energy and total Reynolds stresses

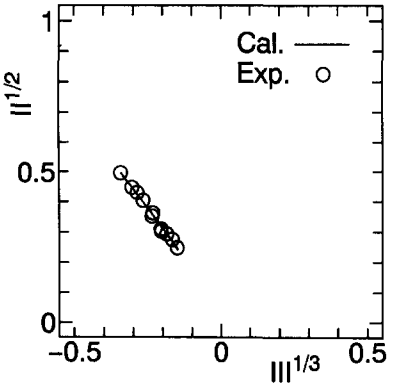

(b)Invariant map

Figure 5 Comparison of numerical results with experiments (data: Le Penven et al. 1985, $III < 0$)

where

$$S_{ij} = \frac{1}{2}\left(\frac{\partial U_i}{\partial x_j} + \frac{\partial U_j}{\partial x_i}\right), \qquad \omega_{ij} = \frac{1}{2}\left(\frac{\partial U_i}{\partial x_j} - \frac{\partial U_j}{\partial x_i}\right) \tag{40}$$

In a multiple-time-scale Reynolds stress model, it may be possible to include nonlinear terms. However, to do so would require the inclusion of too many coefficients, and it becomes impossible for them to be determined. In addition, nonlinear effects of the anisotropy tensor are of secondary importance in the flow when the anisotropy is not large. Therefore, a linear model was adopted as the first step of my study.

It was assumed that the rapid term model in the energy transfer rate equations is proportinal to that in Reynolds stress equations. This assumption is the same as that proposed in the modeling of dissipation rate equations by Tagawa et al. (1991).

Considering the points described above, the governing equations for flow displaying homogeneous shear are modeled as follows:

$$\frac{\partial R_{ij}^{(m)}}{\partial t} = P_{ij}^{(m)} + T_{ij}^{(m-1)} - T_{ij}^{(m)} + \Phi_{S_{ij}}^{(m)} + \Phi_{R_{ij}}^{(m)} \tag{41}$$

$$\frac{\partial T_{ij}^{(m)}}{\partial t} = \alpha_1^{(m)}\frac{T^{(m)}}{e^{(m)}}P_{ij}^{(m)} + \alpha_2^{(m)}\frac{T^{(m)}T^{(m-1)}}{e^{(m)}} - \alpha_3^{(m)}\frac{T^{(m)}T^{(m)}}{e^{(m)}} + \Phi_{TS_{ij}}^{(m)} + \Phi_{TR_{ij}}^{(m)} \tag{42}$$

where

$$P_{ij}^{(m)} = -R_{jk}^{(m)}\frac{\partial U_i}{\partial x_k} - R_{ik}^{(m)}\frac{\partial U_j}{\partial x_k} \tag{43}$$

$$\Phi_{S_{ij}}^{(m)} = -C_1^{(m)}T^{(m)}a_{ij}^{(m)} + C_2^{(m)}T^{(m)}\left(a_{ik}^{(m)}a_{jk}^{(m)} - \frac{1}{3}II^{(m)}\delta_{ij}\right) \tag{44}$$

$$\Phi_{R_{ij}}^{(m)} = C_3^{(m)}e^{(m)}S_{ij} + C_4^{(m)}e^{(m)}\left(a_{ik}^{(m)}S_{jk} + a_{jk}^{(m)}S_{ik} - \frac{2}{3}a_{kl}^{(m)}S_{kl}\delta_{ij}\right) + C_5^{(m)}e^{(m)}\left(a_{ik}^{(m)}\omega_{jk} + a_{jk}^{(m)}\omega_{ik}\right) \tag{45}$$

$$\Phi_{TS_{ij}}^{(m)} = -\alpha_4^{(m)}\frac{T^{(m)}T^{(m)}}{e^{(m)}}a_{T_{ij}}^{(m)} + \alpha_5^{(m)}\frac{T^{(m)}T^{(m)}}{e^{(m)}}\left(a_{T_{ik}}^{(m)}a_{T_{jk}}^{(m)} - \frac{1}{3}II_T^{(m)}\delta_{ij}\right) \tag{46}$$

$$\Phi_{TR_{ij}}^{(m)} = \alpha_6^{(m)}\frac{T^{(m)}}{e^{(m)}}\Phi_{R_{ij}}^{(m)} \tag{47}$$

Determination of model coefficients

Relationships between model coefficients $C_i^{(m)}$. The rapid-term model includes eight coefficients $C_i^{(m)}$ and $\alpha_6^{(m)}$. They

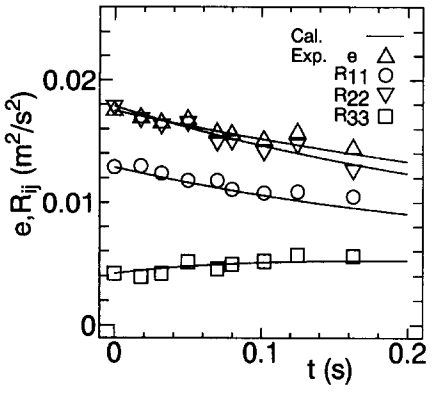

(a)Total turbulent kinetic energy and total Reynolds stresses

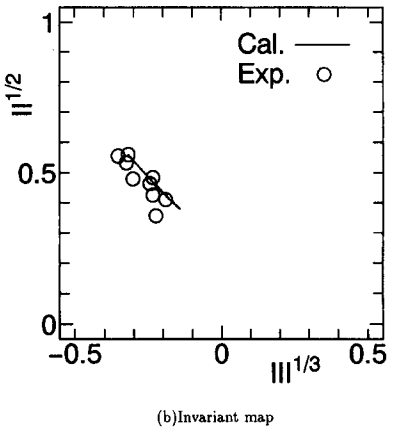

(b)Invariant map

Figure 6 Comparison of numerical results with experiments (data: Tucker and Reynolds 1968, $III < 0$)

were determined by using the experimental data for homogeneous shear flow. The experimental researches have been reported in detail by Rose (1966), Champagne et al. (1970), Mulhearn and Luxton (1975), Harris et al. (1977), Tavoularis and Corrsin (1981), Karnik and Tavoularis (1983), and Rohr et al. (1988). In the former three cases, weak shear causes turbulence to approach an asymptotic state, while in the latter four case strong shear causes turbulence to increase exponentially. Because the temporal changes of Reynolds stresses are zero in the asymptotic state, it is easy to treat this situation analytically, and it is very convenient to use this case to determine model coefficients. Therefore, I decided to use this asymptotic state to determine the model coefficients. The basic procedure is similar to that of Launder et al. (1975). The experimental data used for the purpose are those of Champagne et al., recommended by Ferziger (1981).

First, I derive the relationships between model coefficients $C_i^{(m)}$ analytically. Here, let us consider homogeneous shear flow where a mean velocity exists in the x_1 direction, and a gradient exists in the x_2 direction. Assuming the turbulence reaches an asymptotic state due to the weak shear, the following relations can be expected for the turbulent kinetic energy transfer.

$$P^{(1)} = T^{(1)}, \qquad P^{(1)} + P^{(2)} = T^{(2)} \tag{48}$$

In addition, assuming that the anisotropy of small scale Reynolds stresses is s times that of those for large-scales and that the anisotropy of energy transfer rates is nearly the same as that of Reynolds stresses, the anisotropy tensors $a_{ij}^{(m)}$, Reynolds stresses $R_{ij}^{(m)}$, and energy transfer rates $T_{ij}^{(m)}$ in each spectral slice can be represented as follows:

$$a_{ij}^{(1)} = \left(\frac{1+r}{1+rs}\right) a_{ij} \tag{49}$$

$$a_{ij}^{(2)} = \left(\frac{1+r}{1+rs}\right) s a_{ij} \tag{50}$$

$$R_{ij}^{(1)} = \left(\frac{1+r}{1+rs} a_{ij} + \frac{2}{3}\delta_{ij}\right) \frac{e}{1+r} \tag{51}$$

$$R_{ij}^{(2)} = \left(\frac{1+r}{1+rs} s a_{ij} + \frac{2}{3}\delta_{ij}\right) \frac{re}{1+r} \tag{52}$$

$$T_{ij}^{(1)} = \left(\frac{1+r}{1+rs} a_{ij} + \frac{2}{3}\delta_{ij}\right) \frac{T^{(2)}}{\beta} \tag{53}$$

$$T_{ij}^{(2)} = \left(\frac{1+r}{1+rs} s a_{ij} + \frac{2}{3}\delta_{ij}\right) T^{(2)} \tag{54}$$

On the other hand, by decomposing the total anisotropy tensor a_{ij}, we obtain

$$a_{ij} = \frac{R_{ij}}{e} - \frac{2}{3}\delta_{ij} = \frac{1}{1+r} a_{ij}^{(1)} + \frac{r}{1+r} a_{ij}^{(2)} \tag{55}$$

Using these relations and arranging Equation 41, the total anisotropy tensors can be represented with model coefficients.

$$a_{11} = \left[\frac{4}{3} - \frac{C_4^{(1)}}{3} - C_5^{(1)} + C_2^{(1)}\left(a_{11}^{(1)2} + a_{12}^{(1)2} - \frac{II^{(1)}}{3}\right)\right] / \left[(1+r)\left(1 + C_1^{(1)}\right)\right] + \left[r\left(\frac{4}{3} - \frac{C_4^{(2)}}{3} - C_5^{(2)}\right)\left(1 - \frac{1}{\beta}\right)\right] / \left[(1+r)\left(1 + C_1^{(2)} - \frac{1}{s\beta}\right)\right] \tag{56}$$

$$a_{22} = \left[-\frac{2}{3} - \frac{C_4^{(1)}}{3} + C_5^{(1)} + C_2^{(1)}\left(a_{12}^{(1)2} + a_{22}^{(1)2} - \frac{II^{(1)}}{3}\right)\right] / \left[(1+r)\left(1 + C_1^{(1)}\right)\right] + \left[r\left(-\frac{2}{3} - \frac{C_4^{(2)}}{3} + C_5^{(2)}\right)\left(1 - \frac{1}{\beta}\right)\right] / \left[(1+r)\left(1 + C_1^{(2)} - \frac{1}{s\beta}\right)\right] \tag{57}$$

$$a_{33} = \left[-\frac{2}{3} + \frac{2C_4^{(1)}}{3} + C_2^{(1)}\left(a_{33}^{(1)2} - \frac{II^{(1)}}{3}\right)\right] / \left[(1+r)\left(1 + C_1^{(1)}\right)\right] + \left[r\left(-\frac{2}{3} + \frac{2C_4^{(2)}}{3}\right)\left(1 - \frac{1}{\beta}\right)\right] / \left[(1+r)\left(1 + C_1^{(2)} - \frac{1}{s\beta}\right)\right] \tag{58}$$

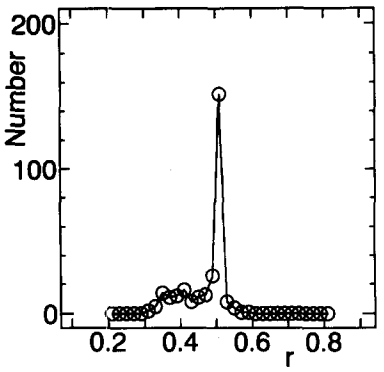

Figure 7 Number of sets that satisfy Equations 56–59

$$a_{12} = \left[a_{22}^{(1)} + \frac{2}{3} - \frac{C_3^{(1)}}{2} - \frac{C_4^{(1)}}{2}\left(a_{11}^{(1)} + a_{22}^{(1)}\right) - \frac{C_5^{(1)}}{2}\left(a_{22}^{(1)} - a_{11}^{(1)}\right) \right] / \left\{ \left[(1+r)\left(1 + C_1^{(1)} - C_2^{(1)}\left(a_{11}^{(1)} + a_{22}^{(1)}\right)\right] a_{12}^{(1)} \right\} + \left\{ r \left[a_{22}^{(2)} + \frac{2}{3} - \frac{C_3^{(2)}}{2} - \frac{C_4^{(2)}}{2}\left(a_{11}^{(2)} + a_{22}^{(2)}\right) - \frac{C_5^{(2)}}{2}\left(a_{22}^{(2)} - a_{11}^{(2)}\right) \right] \left(1 - \frac{1}{\beta}\right) \right\} / \left[(1+r)\left(1 + C_1^{(2)} - \frac{1}{s\beta}\right) a_{12}^{(2)} \right] \quad (59)$$

The model coefficients are to be determined so that these equations agree with the experimental data.

Determination of energy ratio in the asymptotic state. The energy ratio in the asymptotic state must be estimated before determining model coefficients.

The experiment performed by Champagne et al. (1970) indicates that the magnitudes of anisotropy tensor elements are as follows:

$$a_{11} = 0.30, \quad a_{22} = -0.18, \quad a_{33} = -0.12, \quad a_{12} = -0.33 \quad (60)$$

Varying the energy ratio r from 0.2 to 0.8 by increments of 0.02 and $C_3^{(m)}$, $C_4^{(m)}$, and $C_5^{(m)}$ from 0.0 to 2.0 by increments of 0.2, I determined those sets that satisfy Equations 56–59 to within ± 0.015 (i.e., $\pm 5\%$ of a_{11}). On the right-hand sides of Equations 56–59, the unknown variables, except for model coefficients, were given by Equations 38, 49, and 50. The numerical ranges used in the calculation were determined by a priori test with a wider range ($-5.0 \sim 5.0$) and a larger increment (0.5). The numbers of sets are shown in Figure 7. It is obvious that such sets exist from $r = 0.3$ to 0.6, and there is a peak around $r = 0.5$. This fact suggests that stable sets which are not strongly dependent on changes in model coefficients exist around the peak. Although Equations 56–59 are derived using a number of assumptions and approximations, it is reasonable to expect that the asymptotic value of r exists near this peak. Therefore, I assumed that the energy ratio r takes the value 0.5 in the asymptotic state of a homogeneous shear flow.

Coefficients $\alpha_1^{(m)}$. These model coefficients were determined by using the contracted equation forms of Equations 41 and 42. They are expressed as:

$$\frac{\partial e^{(1)}}{\partial t} = P^{(1)} - T^{(1)} \quad (61)$$

$$\frac{\partial e^{(2)}}{\partial t} = P^{(2)} + T^{(1)} - T^{(2)} \quad (62)$$

$$\frac{\partial T^{(1)}}{\partial t} = \alpha_1^{(1)} \frac{T^{(1)}}{e^{(1)}} P^{(1)} - \alpha_3^{(1)} \frac{T^{(1)}}{e^{(1)}} T^{(1)} \quad (63)$$

$$\frac{\partial T^{(2)}}{\partial t} = \alpha_1^{(2)} \frac{T^{(2)}}{e^{(2)}} P^{(2)} + \alpha_2^{(2)} \frac{T^{(2)}}{e^{(2)}} T^{(1)} - \alpha_3^{(2)} \frac{T^{(2)}}{e^{(2)}} T^{(2)} \quad (64)$$

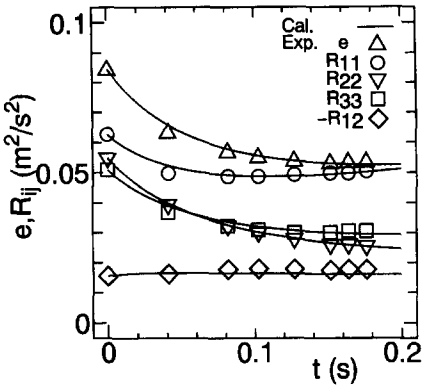

(a)Total turbulent kinetic energy and total Reynolds stresses

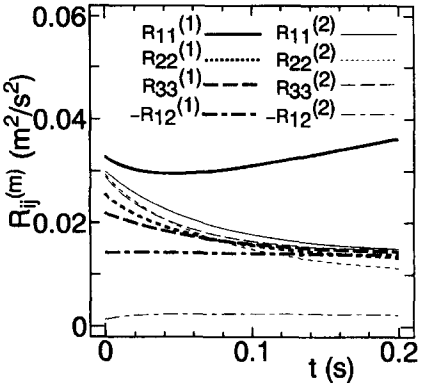

(b)Large and small-scale Reynolds stresses

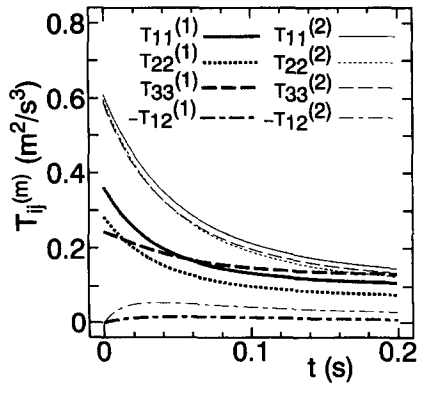

(c)Large and small-scale energy transfer rates

Figure 8 Comparison of numerical results with experiments (data: Champagne et al. 1970)

Assuming the asymptotic state, and using Equations 61–64, the following relations can be obtained.

$$\alpha_1^{(1)} = \alpha_3^{(1)}, \qquad \alpha_1^{(2)} = \frac{\beta}{\beta - 1}\left(\alpha_3^{(2)} - \frac{\alpha_2^{(2)}}{\beta}\right) \tag{65}$$

Since I set $r = 0.5$ in the asymptotic state, Equations 24 and 38 leads to $\alpha_3^{(1)} = 0.9$; $\alpha_3^{(2)} = 1.4$; $\alpha_2^{(2)} = 1.05$; and $\beta = 1.3$. Substituting these values into Equation 65, model coefficients $\alpha_1^{(m)}$ can be obtained as follows:

$$\alpha_1^{(1)} = 0.9, \qquad \alpha_1^{(2)} = 2.6 \tag{66}$$

Although the production in the small scale $P^{(2)}$ is included in the model, this fact does not force $P^{(2)}$ to be large in the equilibrium state. In fact, $P^{(1)} \approx T^{(1)} \approx T^{(2)}$ and $P^{(2)} \approx 0$ were realized in my calculations.

Coefficients $C_i^{(m)}$ and $\alpha_6^{(m)}$. The remaining coefficients were determined through computational optimization. The sets of model coefficient values which were obtained in the determination of the asymptotic energy ratio were used in conjunction with the experimental data measured by Champagne et al. (1970). I sought a set consistent with the experimentally observed behavior, for example R_{22} intersects R_{33} during the change. Finally, I adopted following values.

$$C_3^{(1)} = 0.5, \quad C_4^{(1)} = 1.2, \quad C_5^{(1)} = 0.4, \quad \alpha_6^{(1)} = 1.4$$
$$C_3^{(2)} = 1.0, \quad C_4^{(2)} = 0.5, \quad C_5^{(2)} = 0.7, \quad \alpha_6^{(2)} = 2.5 \tag{67}$$

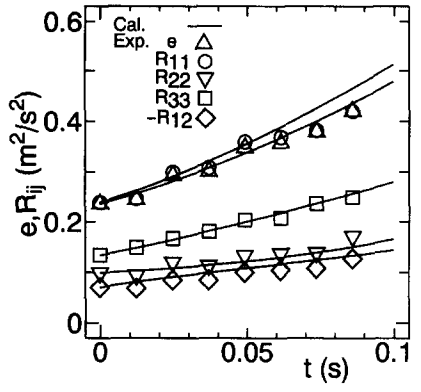

(a)Total turbulent kinetic energy and total Reynolds stresses

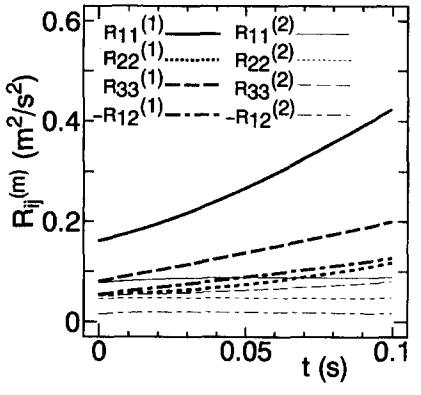

(b)Large and small-scale Reynolds stresses

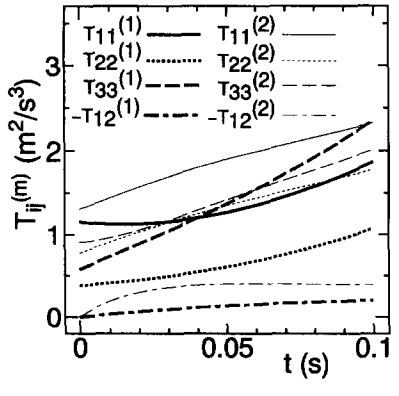

(c)Large and small-scale energy transfer rates

Figure 9 Comparison of numerical results with experiments (data: Harris et al. 1977)

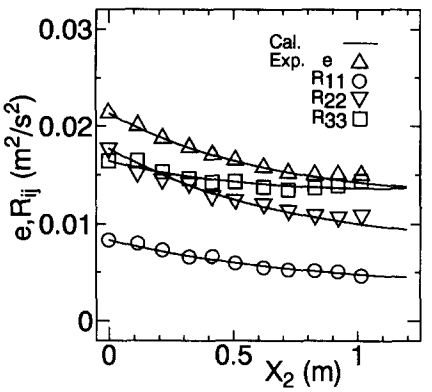

(a)Total turbulent kinetic energy and total Reynolds stresses

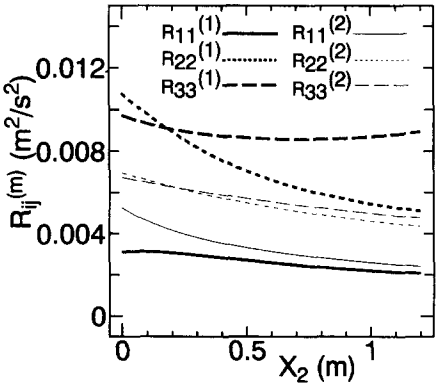

(b)Large and small-scale Reynolds stresses

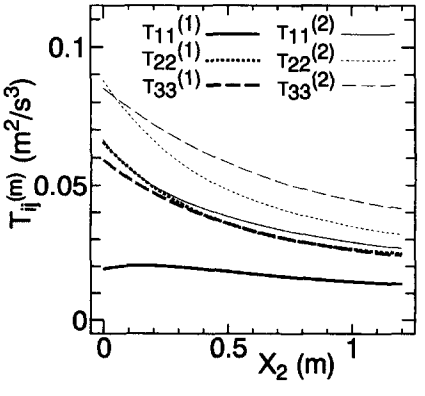

(c)Large and small-scale energy transfer rates

Figure 10 Comparison of numerical results with experiments (data: Tucker and Reynolds 1968)

Initial conditions and numerical method

The numerical procedure here is similar to that used in the simulation of grid turbulence (see *Initial conditions and numerical method* section). However, two points are different. One is that the shear component of the energy transfer rates was assumed to be zero in the initial state. This is because the dissipation of shear Reynolds stress is one order smaller than that of normal Reynolds stress. The second point is that the Reynolds stress components were found by interpolating the experimental data used in estimating the energy ratio r (i.e., *Step II*).

Results and discussion

Three homogeneous shear flows were considered, and the numerical results were compared with experimental data. The first case is the weak shear flow studied by Champagne et al. (1970). This case is the base data used in the determination of model coefficients in the rapid terms. In their experiment, the strain rate is 12.9 (1/s), and the turbulence reaches an asymptotic state. The second case is the strong shear flow investigated by Harris et al. (1977). In this case, the shear rate is 44.0 (1/s), and the turbulence grows exponentially. The third case is the distorting duct flow measured by Tucker and Reynolds (1968). In this case, mean velocity gradients exist in two directions. These data were recommended by Ferziger (1981) in the Stanford Conference.

Figure 8 shows the numerical results for the first case. Figure 8a displays the behavior of the total turbulent kinetic energy and total Reynolds stresses. The total turbulent kinetic energy is governed by the contracted equations, and only the initial energy ratio influences the terminal level. Therefore, its time evolution depends on the model coefficients $\alpha_1^{(m)}$, $\alpha_2^{(m)}$, and $\alpha_3^{(m)}$. The relative level of Reynolds stresses is governed by rapid terms. As the numerical results are in good agreement with the experiment, it is apparent that the coefficients adopted in the present model are reasonable. Figure 8b shows the temporal change of each Reynolds stress in a large- and a small-scale region. Each component of large-scale turbulence behaves differently. $R_{11}^{(1)}$ increase due to the production. Other normal components decrease, and the shear component remains constant. On the other hand, small-scale components decrease monotonically and are nearly isotropic. Figure 8c shows the energy transfer rates. Large-scale components do not evolve toward isotropy, while small-scale ones are nearly isotropic. Shear components are negative here and much smaller than normal ones. This characteristic is the same as that assumed in single-time-scale models and the direct numerical simulation (DNS) results. Although the excellent agreement with experiment is a matter of course, since the model coefficients are determined by referring to these data, the discrepancies between the large- and small-scale motion are very interesting.

Figure 9 shows the numerical results for the second case (Harris et al. 1977), where the shear is strong. It is known that single-time-scale models overestimate the turbulent kinetic energy. Figure 9a shows that the present model can capture the behavior satisfactorily, although R_{11} is slightly overestimated. Figure 9b shows the time evolution of the partitioned Reynolds stresses. All large-scale components increase rapidly due to the strong shear, while small-scale ones remain nearly constant. This result suggests that production mainly contributes to large-scale motion, and the rapid change does not produce an immediate effect on small-scale Reynolds stresses. Figure 9c shows the energy transfer rates. $T_{33}^{(1)}$ increases drastically because of the large redistribution from $R_{11}^{(1)}$. Also, small-scale components increase rapidly. This reflects the fact that large production causes dissipation to increase.

Figure 10 shows the results for the turbulence through a distorting duct measured by Tucker and Reynolds (1968). Nearly homogeneous turbulence is subjected to three strain components (i.e., $\partial U_1/\partial x_1 = -1/2\partial U_2/\partial x_2 = \partial U_3/\partial x_3 \neq 0.0$). For this case, I considered only the region where the axial velocity U_2 is nearly constant in the duct. The agreement of the numerical results with the experiment is quite good (Figure 10a). The behavior of partitioned Reynolds stresses and energy transfer rates are shown in Figures 10b and c. They are similar to those in the weak shear case.

From these calculations, it is verified that the present model can satisfactorily reproduce homogeneous shear flows under different conditions without rearranging model coefficients.

Conclusion

A multiple-time-scale Reynolds stress model was investigated. The basic forms of model equations were introduced and applied to grid turbulence and homogeneous shear flow. The model coefficients, mainly concerned with pressure–strain correlation, were determined analytically and/or numerically. In addition, the present model was verified for five sets of experimental data for grid turbulence with different initial conditions and two homogeneous shear flows subjected to different mean velocity gradients. It was shown that the present model can satisfactorily reproduce all data without adjusting model coefficients and that the method used to set initial conditions is reasonable for a wide range of turbulence.

Acknowledgment

This research has been supported through the Grant-in-Aid for Scientific Research (No. 05240220 and No. 06231216) by the Ministry of Education, Science, and Culture.

References

Champagne, F. H., Harris, V. G. and Corrsin, S. 1970. Experiments on nearly homogeneous turbulent shear flow. *J. Fluid Mech.*, **41**, 81–139

Gence, J. N. and Mathieu, J. 1979. On the application of successive plane strains to grid-generated turbulence. *J. Fluid Mech.*, **93**, 501–513

Hanjalic, K., Launder, B. E. and Schiestel, R. 1980. Multiple-time-scale concepts in turbulent transport modelling. In *Turbulent Shear Flows 2*, L. J. S. Bradbury, et al. (eds.), Springer-Verlag, Berlin, 36–49

Harris, V. G., Graham, J. A. H. and Corrsin, S. 1977. Further experiments in nearly homogeneous turbulent shear flow. *J. Fluid Mech.*, **81**, 657–687

Jeandel, D., Brison, J. F. and Mathieu, J. 1978. Modeling methods in physical and spectral space. *Phys. Fluids*, **21**, 169–182

Karnik, U. and Tavoularis, S. 1983. The asymptotic development of nearly homogeneous turbulent shear flow. *Proc. 4th Symposium on Turbulent Shear Flows*, 14.18–14.23

Kim, S. W. and Chen C. P. 1987. A multiple-time-scale turbulence model based on variable partitioning of turbulent kinetic energy spectrum. NASA CR-179222

Kim, S. W. 1988. A near-wall turbulence model and its application to fully developed turbulent channel and pipe flows. NASA TM-101399

Kim, S. W. and Chen, C. P. 1989. A two-layer multiple-time-scale turbulence model and grid independence study. NASA CR-183653

Kim, S. W. 1991. Calculation of divergent channel flows with a multiple-time-scale turbulence model. *AIAA J.*, **29**, 547–554

Ferziger, J. H. 1981. In *Proceedings of 1980–81 AFOSR-HTTM Stanford Conf. Complex Turbulent Shear Flows*, S. J. Kline, et al. (eds.), Stanford University, California, 405–433

Launder, B. E., Reece, G. J. and Rodi, W. 1975. Progress in the development of a Reynolds-stress turbulence closure. *J. Fluid Mech.*, **68**, 537–566

Le Penven, L., Gence, J. N. and Comte-Bellot, G. 1985. On the approach to isotropy of homogeneous turbulence: Effect of the partition of kinetic energy among the velocity components. In *Frontiers in Fluid Mechanics*, S. H. Davis, and J. L. Lumley, (eds.), Springer-Verlag, Berlin, 1–21

Lumley, J. L. and Newman, G. R. 1977. The return to isotropy of homogeneous turbulence. *J. Fluid Mech.*, **82**, 161–178

Makita, H., Minami, K. and Murao, T. 1993. Decay and return to isotropy process of homogeneous three-dimensionally anisotropic turbulence. *Proc. 71st JSME Fall Annual Meeting*, 57–59 (in Japanese)

Mulhearn, P. J. and Luxton, R. E. 1975. The development of turbulence structure in a uniform shear flow. *J. Fluid Mech.*, **68**, 577–590

Rohr, J. J., Itsweire, E. C., Helland, K. N. and Van Atta, C. W. 1988. An investigation of the growth of turbulence in a uniform-mean shear flow. *J. Fluid Mech.*, **187**, 1–33

Rose, W. G. 1966. Results of an attempt to generate a homogeneous turbulent shear flow. *J. Fluid Mech.*, **25**, 97

Schiestel, R. 1987. Multiple-time-scale modeling of turbulent flows in one point closure. *Phys. Fluids*, **30**, 722–731

Schumann, U. 1977. Realizability of Reynolds-stress turbulence models. *Phys. Fluids*, **20**, 721–725

Speziale, C. G., Sarkar, S. and Gatski, T. 1991. Modelling the pressure–strain correlation of turbulence: An invariant dynamical systems approach. *J. Fluid Mech.*, **227**, 245–272

Tagawa, M., Nagano, Y. and Tsuji, T. 1991. Turbulence model for the dissipation components of Reynolds stresses. *Proc. 8th Symp. on Turbulent Shear Flows*, 29–3

Tavoularis, S. and Corrsin, S. 1981. Experiments in nearly homogeneous turbulent shear flow with a uniform mean temperature gradient. *J. Fluid Mech.*, **104**, 311–347

Tucker, H. J. and Reynolds, A. J. 1968. The distortion of turbulence by irrotational plane strain. *J. Fluid Mech.*, **32**, 657–673

Wilcox, D. C. 1986. Multiscale model for turbulent flows. AIAA Paper 86–29

Wilcox, D. C. 1988. Multiscale model for turbulent flows. *AIAA J.*, **26**, 1311–1320

Yamamoto, M. and Arakawa, C. 1991. Study on the pressure–strain term in Reynolds stress model. *Proc. 8th Symp. on Turbulent Shear Flows*, III-17-1-III-17-2.